Phase transitions and self-organization of Janus disks in two dimensions studied by Monte Carlo simulations

M. Borówko and W. Rżysko

Department for the Modelling of Physico-Chemical Processes, M. Curie-Skłodowska University, 20-031 Lublin, Poland

(Received 23 April 2014; revised manuscript received 11 September 2014; published 15 December 2014)

The phase behavior of Janus disks on a square lattice is studied using the Monte Carlo method. A particle is composed of two different parts, A and B. The interactions between neighboring particles depend on their orientations. To control the strength of the interactions, we use energy parameters characterizing AA, BB, and AB contacts. The phase diagrams are estimated. We found two phase transitions, namely first-order transitions between colloidal-rich and colloidal-poor phases, and continuous order-disorder transitions to different ordered phases. A variety of ordered structures occurs depending on the relation between the energy parameters and on the fluid density. The influence of energy parameters on the phase diagram topology and critical parameters is shown. The competition between phase transitions and self-organization is discussed.

DOI: 10.1103/PhysRevE.90.062308 PACS number(s): 64.75.Xc, 68.35.Rh, 64.75.Yz

I. INTRODUCTION

The application of particles with controlled anisotropy to the fabrication of new materials with desirable functionality is central in today's research. The molecular engineering is based on their intrinsic property to self-assemble under certain thermodynamic conditions. Understanding the principles of self-organization and phase behavior is necessary to control the formation of assembled structures. This problem has attracted increasing attention due to promising applications of the new materials in nanotechnology, biotechnology, electronics, photonics, drug delivery, and others [1,2].

A great variety of particles exhibit a tendency to self-organize. A prominent example is a broad class of Janus-like particles that are composed of at least two chemically or physically distinctive parts. Such particles can be divided into several classes according to their architecture and dimensionality. Numerous works have been devoted to study spherical Janus particles that interact via different anisotropic potentials. The first example is provided by "the classical" Janus particle, i.e., a sphere with one-half of the surface being hydrophilic whereas the other remained hydrophobic [3]. They can provide the most elementary model of surfactants [4]. Another interesting class of particles are so-called patchy particles that involve localized surface areas exerting attractive forces [2]. Recently, Janus-like particles of different shapes have been investigated [5,6]. Kraft *et al.* [7] have proposed a new "patchy model," in which Janus dimers consisted of one rough and one smooth sphere. The binary-mixture model of Janus fluids with up-down constrained orientations has also been considered [8,9]. This model refers to the fluid in an external static electrical field.

Over the past few years, the collective behavior of Janus particles has been intensively investigated. A goal of numerous works was to find the interconnection between individual particle properties and the resulting self-assembled structures. For this purpose, Monte Carlo [6–16] and molecular-dynamic methods [17,18] have often been used. Computer simulations have been supplemented by various theoretical approaches. Among these are simple analytical [8,9], Ginzburg-Landau [19,20], density functional [21–23], integral equation [8,9,24,25], and thermodynamic perturbation theories [25,26].

The directional dependence of interactions between Janus particles leads to rich phase behavior and self-assembly into various aggregates and mesoscale structures [2,3,6–26]. Erdmann *et al.* [10] investigated the phase behavior of Janus beads. In this model, different orientations of particles are preferred depending on the assumed parameters of the anisotropic potential. As a consequence, various ordered phases were observed. Sciortino *et al.* [12,13] studied the one-patchy particles in the framework of the Kern-Frenkel model [11]. They found various aggregation structures, such as micelles, vesicles, and bilayers. Their studies have shown the existence of the first-order condensation transition. They observed the coexistence of a dilute phase of micelles and a denser phase of larger clusters. The demixing region is progressively suppressed by the insurgence of micelles. The authors discussed the competition between the self-assembly and phase separation. In the framework of the model of binary-mixture Janus fluids with up-down constrained orientations, a gas-liquid transition under global equimolar conditions and the demixing transitions have been analyzed for selected systems [8,9]. It has been shown that the imposed constraints in the attractive patch orientations inhibit the formation of the inert clusters, which in the original Janus fluid [12,13] were responsible for a reentrant gas branch. Moreover, anisotropies in the geometry of particles, as well as in the properties of interactions, give rise to a rich phase behavior of colloidal systems [6]. Phase separation and self-assembly of colloidal dimers with tunable attractive strengths have been discussed by Munao *et al.* [6]. In the limit of Janus dumbbells, the formation of lamellar structures, preempting the gas-liquid phase separation, has been observed. In addition to the condensation transition, the crystallization of the Janus particles was investigated using a wide range techniques. It has been shown that the simple Janus beads formed stable crystal structures with complicated bond topologies [14].

The behavior of nanoparticles at interfaces has been studied from a fundamental point of view and exploited in applications [27,28]. Intensive work has been done to understand the effects of Janus particles at liquid-liquid interfaces [29–31] and their behavior near solid surfaces [21–23]. Janus particles can form two-dimensional films at interfaces. Such monolayers can be

obtained, for example, from amphiphilic disklike molecules adsorbed onto a solid surface, with particle-substrate interactions rendering the disk coplanar to the surface [32–34]. Because of possible applications, the self-assembly of Janus particles in two-dimensional systems is an important topic in colloid science.

It is well known that complex molecules adsorbed on solid surfaces can form regular patterns and exhibit a rich phase behavior. Therefore, numerous papers have been devoted to study phase transitions in adsorbed layers formed on surface lattices [35]. In particular, extensive Monte Carlo simulations have been carried out for monolayers consisting of heterogeneous dimers, i.e., linear molecules built out of two chemically distinct segments [36–40]. Two simple models have been considered. In the first, all dimers were adsorbed parallel to the surface [36–38], whereas in the second they assumed perpendicular orientation [39,40]. The results reveal a great variety of vapor-liquid coexistence behaviors depending on the relative strengths of interactions between molecule segments. In the case of heterogeneous dimers, the phase diagrams included many challenging features, such as triple points, tricritical points, or end-critical points. Apart from the vapor-liquid transition, liquid-liquid coexistence has been found [36–38]. The occurrence of spontaneous, orientational ordering in the liquid was demonstrated. The evolution of phase diagrams with a change of the model parameters has been discussed. Recent studies [18] have shown that also Janus disks in two-dimensional systems self-organized in a number of mesophases of various symmetries with a variety of novel patterns.

In this paper, we present computer simulation for Janus disks adsorbed on a square lattice. In contrast to numerous works [10–16,21–26], we have introduced the simple lattice model. Monte Carlo simulations in lattice systems are considerably less time-consuming than those for continuous models. In this way, one can effectively scan the space of the model parameters.

We propose here a simple model for the anisotropic interactions between Janus disks. The potential is a linear combination of three parameters characterizing the strengths of interactions between the same and unlike parts of the disks. The interaction between particles depends on their orientations. Depending on the relations between the energy parameters, our model reduces to the two-dimensional lattice version of the Kern-Frenkel model [11] or models for amphiphilic particles [17]. We consider different sets of the energy parameters. This enables us to simulate various kinds of systems. In contrast to heterogeneous dimers, the Janus disks occupied only one lattice site. The model involves the anisotropy in the interactions but not in the particle shape. Therefore, the phase behavior of Janus disks and heterogeneous dimers is considerably different.

The aim of our computer simulations is to show the effects of differences in strengths of interactions between particular parts of Janus disks on the nature of self-organization and phase transitions. We want to study general trends of phase behavior of the model. First of all, we discuss the ground-state properties and analyze ordered structures generated by the model. Next, we want to explain how the choice of energy parameters affects the topology of phase diagrams and critical parameters of condensation for selected systems. We show that our model captures important features of self-assembly and phase separation in the system.

From a theoretical point of view, it is also interesting to investigate the behavior of Janus objects in the systems with lower dimensionality and the symmetry imposed by the substrate. The results can be utilized for the production of patterned surface structures.

II. MODEL

We consider Janus disks on a simple square lattice. The fluid molecules are circular plates composed of two different halves, A and B. They are located parallel to the lattice plane. Each lattice site may be occupied or remain empty. For simplicity, we assume that a particle may take only four orientations, as presented in Fig. 1(a). In the case of orientations labeled as 1 and 2 (3 and 4), the diameter that divides two different parts of a particle is parallel (perpendicular) to the x axis. The particle can be treated as a unit vector perpendicular to the dividing diameter and oriented from B to A. The possible orientations correspond to the following vectors: $\mathbf{v}^{(1)} = (0,1)$, $\mathbf{v}^{(2)} = (0,-1)$, $\mathbf{v}^{(3)} = (1,0)$, and $\mathbf{v}^{(4)} = (-1,0)$.

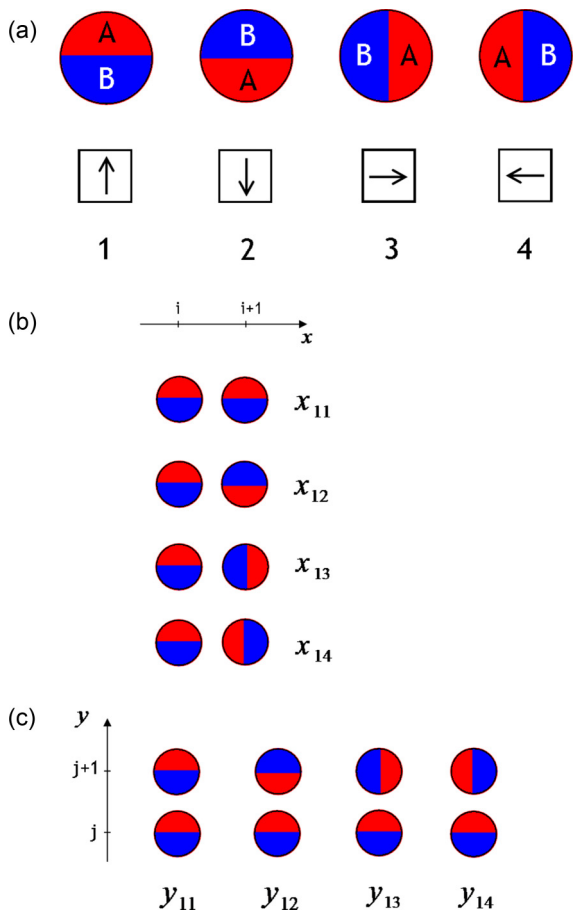

FIG. 1. (Color online) Orientations of the model Janus disks (a), and representative examples of pairs x_{k1} (b) and y_{k1} (c). For pairs x_{k1} (y_{k1}), the lines connecting the centers of the particles are aligned along the x (y) axis. The indexes indicate the orientations of particles located on sites with the successive x (y) coordinates.

We introduced the generalized gas-lattice model. To each site we assigned a set of occupation variables $(c1_i, c2_i, c3_i, c4_i)$ that are equal to unity (zero) when the site is occupied by a particle with the kth orientation (when it is empty or occupied by a particle with orientation different from the kth orientation),

$$ck_i = \begin{cases} 1 & \text{for the } k\text{th orientation,} \\ 0 & \text{otherwise.} \end{cases} \tag{1}$$

We can also use the total occupation variable c_i defined as the sum of occupation variables ck_i,

$$c_i = \sum_{k=1}^{4} ck_i = \begin{cases} 1 & \text{for an occupied site,} \\ 0 & \text{for an empty site.} \end{cases} \tag{2}$$

Then we assume that a pair of particles interacts one with another whenever they occupy the first-nearest neighboring sites. The interaction energy between particles i and j depends on their orientations $\mathbf{v}_i, \mathbf{v}_j$ and on the particle separation vector $\mathbf{r}_{ij}$ $(|\mathbf{r}_{ij}| = 1)$, $u = u(\mathbf{v}_i, \mathbf{v}_j, \mathbf{r}_{ij})$. To characterize a configuration of a pair, one can use the following scalar products: $v_{ij} = \mathbf{v}_i \cdot \mathbf{v}_j$, $w_{ij} = \mathbf{r}_{ij} \cdot \mathbf{v}_j$, and $w_{ji} = \mathbf{r}_{ji} \cdot \mathbf{v}_j$ [11]. In the case of perpendicular vectors, the scalar product $v_{ij} = 0$. For two identical vectors (parallel), $v_{ij} = 1$ while the value $v_{ij} = -1$ corresponds to an antiparallel configuration. We can distinguish 32 types of pairs of interacting particles. Examples of these pairs are shown in Figs. 1(b) and 1(c). For a pair labeled x_{k1} (y_{k1}), the particle separation vector is aligned parallel to the x axis (y axis). The indexes indicate the orientations of particles located on sites with successive x (y) coordinates.

We define three energy parameters: u_{AA}, u_{BB}, and u_{AB}, which characterize interactions between identical and unlike parts of particles in parallel or antiparallel pair configurations. The parameter u_{AA} (u_{BB}) is defined as the interaction energy for a pair in which A (B) parts face each other [e.g., the configuration y_{12} in Fig. 1(c)]. The parameter corresponds to the head-to-tail configuration [e.g., the pair y_{11} in Fig. 1(c)].

We assume that the pair interaction energy, u_l, is the arithmetic average of two energy parameters corresponding to patches being in contact,

$$u_l = \tfrac{1}{2}(u_\alpha + u_\beta), \tag{3}$$

where $\alpha, \beta = AA, BB, AB$. It is easy to show that the definition (3) generates only six possible values of the pair energy u_l. These values are collected in Table I.

To give a link between the heuristic definition (3) and vectors $\mathbf{v}_i, \mathbf{v}_j$, and $\mathbf{r}_{ij}$ characterizing a given pair, we define two variables: $w = w_{ij} + w_{ji}$ and $p = w_{ij} w_{ji}$. We have shown that the energy u_l is univocally determined by the variables v_{ij}, w, and p. This relation is presented in Table I. The pairs corresponding to the energies are shown in the last column.

Notice that in this model different pairs can correspond to the same value u_l. The pair energy states are degenerated. For example, either the pair x_{12} or the pair x_{33} contributes the value u_{AB} to the total potential energy of the system. Moreover, the energies u_1 and u_2 (u_3 and u_4) correspond to antiparallel (parallel) configurations, while the energies u_5 and u_6 correspond to perpendicular configurations.

TABLE I. Pair energies with corresponding values of parameters v_{ij}, w, p and pair configurations.

Energy	v_{ij}	w	p	Pairs
$u_1 = u_{AA}$	-1	2	1	x_{34}, y_{12}
$u_2 = u_{BB}$	-1	-2	1	x_{43}, y_{21}
$u_3 = u_{AB}$	1	0	-1	x_{33}, x_{44}, y_{11}, y_{22},
	-1	0	0	x_{12}, x_{21}, y_{34}, y_{43}
$u_4 = 0.5(u_{AA} + u_{BB})$	1	0	0	x_{11}, x_{22}, y_{33}, y_{44}
$u_5 = 0.5(u_{AA} + u_{AB})$	0	1	0	x_{14}, x_{31}, x_{32}, x_{24},
				y_{32}, y_{42}, y_{13}, y_{14}
$u_6 = 0.5(u_{BB} + u_{AB})$	0	-1	0	x_{13}, x_{41}, x_{42}, x_{23},
				y_{31}, y_{41}, y_{23}, y_{24}

In the grand canonical ensemble, the Hamiltonian of N particles at temperature T can be written as [35]

$$H = \sum_{l=1}^{6} u_l n_l - N\mu, \tag{4}$$

where n_l is a number of pairs that contribute the u_l to the total potential energy of the system. The fluid density can be expressed as

$$\rho = \frac{1}{L^2} N = \frac{1}{L^2} \sum_i c_i, \tag{5}$$

where L is a number of lattice sites. The summation in Eq. (5) is over all lattice sites. In a similar way, we calculate the density of molecules in the kth orientation,

$$\rho_k = \frac{1}{L^2} N_k = \frac{1}{L^2} \sum_i ck_i, \tag{6}$$

where N_k is a number of molecules with the kth orientation.

To investigate phase transitions and ordering in the system, we introduce several order parameters. For a gas-liquid transition, we used the usual parameter defined as

$$m = \rho - \langle \rho \rangle, \tag{7}$$

where $\langle \rho \rangle$ is the ensemble average.

The model predicts the existence of four ordered structures for a fully covered lattice: the superantiferromagnetic (SAF1, SAF2) and antiferromagnetic (AF1, AF2) phases [41]. All these structures are presented in Fig. 2.

We analyze the structural transitions using a standard method proposed for lattice systems [41]. To distinguish the ordered phases, we define the suitable order parameters in the way described below. First, by analogy to the models of magnets, we define the following spin variables:

$$S_{12,i} = \begin{cases} 1 & \text{for } c1_i = 1, \\ -1 & \text{for } c2_i = 1, \\ 0 & \text{otherwise} \end{cases} \tag{8}$$

and

$$S_{34,i} = \begin{cases} 1 & \text{for } c3_i = 1, \\ -1 & \text{for } c4_i = 1, \\ 0 & \text{otherwise.} \end{cases} \tag{9}$$

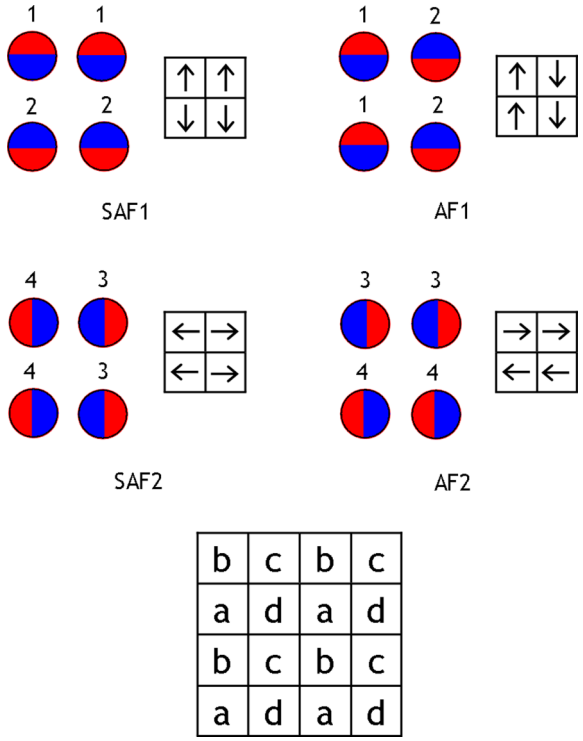

FIG. 2. (Color online) Schematic representation of different possible ordered structures at a fully filled lattice and decomposition of a square lattice into four equivalent sublattices a, b, c, and d.

Second, we decompose the entire lattice into four interpenetrating and equivalent sublattices, as shown in the lower part of Fig. 2, and we introduce the average "magnetizations" of each sublattice α [41],

$$m_{12,\alpha} = \frac{1}{L^2} \sum_{i \in \alpha} S_{12,i} \tag{10}$$

and

$$m_{34,\alpha} = \frac{1}{L^2} \sum_{i \in \alpha} S_{34,i}, \tag{11}$$

where $\alpha = a,b,c,d$.

Using the above sublattice magnetizations, we define the following order parameters:

$$\Psi_{\mathrm{SAF1}} = -m_{12,a} + m_{12,b} + m_{12,c} - m_{12,d}, \tag{12}$$

$$\Psi_{\mathrm{SAF2}} = -m_{34,a} - m_{34,b} + m_{34,c} + m_{34,d}, \tag{13}$$

$$\Psi_{\mathrm{AF1}} = m_{12,a} + m_{12,b} - m_{12,c} - m_{12,d}, \tag{14}$$

$$\Psi_{\mathrm{AF2}} = -m_{34,a} + m_{34,b} + m_{34,c} - m_{34,d}. \tag{15}$$

Finally, we introduce the order parameter suitable to detect the presence of the SAF phase,

$$\Psi_{\mathrm{SAF}} = \sqrt{\Psi_{\mathrm{SAF1}}^2 + \Psi_{\mathrm{SAF2}}^2}, \tag{16}$$

and the order parameter that describes the ordering characteristic for the AF structure,

$$\Psi_{\mathrm{AF}} = \sqrt{\Psi_{\mathrm{AF1}}^2 + \Psi_{\mathrm{AF2}}^2}. \tag{17}$$

Let us discuss briefly the properties of these order parameters. As usual, the order parameter Ψ_{SAF} (Ψ_{AF}) changes from 0 to 1. It achieves the maximum value for a perfectly ordered phase: $\Psi_{\mathrm{SAF}} = 1$ ($\Psi_{\mathrm{AF}} = 1$). In such a phase, the order parameter Ψ_{SAF1} (Ψ_{SAF2}) assumes values 1 or -1. These values correspond to the structures aligned to the x or y axis. Moreover, if $\Psi_{\mathrm{SAF1}} = \pm 1$ ($\Psi_{\mathrm{SAF1}} = \pm 1$), then $\Psi_{\mathrm{SAF2}} = 0$ ($\Psi_{\mathrm{SAF1}} = 0$). The same relations hold for the order parameter Ψ_{AF} and its components Ψ_{AF1},Ψ_{AF2}.

We have calculated also the fourth-order cumulants of the order parameters [42],

$$U(\Psi) = 1 - \frac{\langle \Psi^4 \rangle}{3\langle \Psi^2 \rangle^2}, \tag{18}$$

where Ψ denotes any order parameter. The above-defined quantities can be calculated during Monte Carlo simulation.

It is worthwhile to compare our model with other gas-lattice models. The simplest gas-lattice model has been formulated for a fluid consisting of isotropic molecules. This model can be readily mapped into the two-state Ising model [43]. For anisotropic particles, the model becomes more complex because of a larger number of possible configurations. This means that more variables should be used to characterize a state of a given lattice site. For example, a heterogeneous dimer AB may occupy one or two lattice sites, depending on whether it assumes an orientation parallel or perpendicular to the surface. In the latter case, there are two configurations when different segments (A or B) are in contact with the surface. The monolayer film consisting of the perpendicularly adsorbed dimers AB can be modeled by the spin -1 model in which the spin variable can take three values ± 1 and 0 [35,39,40]. This model was originally proposed by Blume, Emery, and Griffiths [44] to describe the phase behavior of liquid mixtures of helium isotopes. Several versions of spin models have been used to study a variety of problems in condensed-matter physics: orderings in magnets, alloys, mixtures, and fluids in embedded integral degrees of freedom. Under certain conditions, heterogeneous dimers adsorbed parallel to the surface can be studied in the framework of the BEG model [38]. Various more advanced lattice models have also been considered, namely the Heisenberg, XY, and Potts models [43]. In a general case, our approach can be treated as a version of the Potts model.

III. MONTE CARLO METHOD

We have carried out Monte Carlo simulations in the grand canonical ensemble using the hyperparallel tempering technique [45–48]. A square simulation cell was used with standard periodic boundary conditions in both directions. The linear dimensions of the system (L) ranged between 60 and 192. A Monte Carlo step consisted of an attempt to insert a particle into the system at a randomly chosen position or to remove an existing particle. A number of MC steps necessary to obtain solid results depended considerably on the assumed values of the energy parameters. In the majority of simulations, we used 10^9 MC steps (per site) for equilibration and 10^{10} for production runs. However, for certain sets of energy parameters, the simulations had to be substantially

longer. The multiple-histogram reweighting method was used to analyze the results [49,50].

The reordered quantities were the densities of differently oriented particles ρ_k, the total density ρ, the order parameters, and the fourth-order cumulants of the order parameters. We have estimated the histograms of the order parameters. The histograms of the density $p(\rho)$ were used to determine a line of vapor-liquid coexistence. The coexistence was located using the equal peak-weight criterion for the density histogram [46]. The histograms of the remaining order parameters allowed us to identify the ordered structures existing in the considered systems.

For certain systems, the simulations in the grand canonical ensemble became prohibitively long and the interpretation of the results was difficult. Therefore, for a few systems we additionally carried out simulations in the canonical ensemble. We used the block distribution function analysis [51,52]. The simulation cell was divided into smaller subsystems (blocks). We estimated the distribution functions $P(\rho^*)$ that characterize the normalized probability that the system has density ρ^* within a given block.

Finite-size scaling theory was used to study the nature of phase transitions and to estimate critical parameters [53]. In this way we analyzed how the order parameters and their fourth-order cumulants change with varying temperature and the chemical potential for different sizes of the simulation cell. We recall here only the main features of these quantities; for further details, we refer the reader to the literature [35–42,53]. The curves Ψ_L versus T (Ψ_L versus μ) plotted for different linear dimensions of the system have an intersection point as a first-order phase transition occurs. On the contrary, for a continuous phase transition, the curves do not cross one another. The cumulants $U_L(\Psi)$ versus T [$U_L(\Psi)$ versus μ] adopt a nontrivial fixed point $U_L(T_t) = U^*$ [$U_L(\mu_t) = U^*$]. In the case of a first-order transition for a sufficiently large system, a minimum appears on a curve $U_L(\Psi)$ versus T [$U_L(\Psi)$ versus μ]. However, for the second-order transition, the curves are always monotonic. The intersection points of the curves $U_L(\Psi)$ versus T [$U_L(\Psi)$ versus μ] give an accurate estimate of the critical temperature and the critical potential [42]. In this paper, we assume that $|u_{BB}|$ is the unit of energy, the reduced temperature is defined as $T^* = k_B T/|u_{BB}|$, and the reduced chemical potentials are given by $\mu^* = \mu/k_B$.

IV. RESULTS AND DISCUSSION

We begin with a discussion of the preferred configurations generated by our model. A comparison of possible pair energies collected in Table I leads to the conclusion that the energies u_4, u_5, and u_6 are never lower than one of the energies $u_1 = u_{AA}$, $u_2 = u_{BB}$, or $u_3 = u_{AB}$. This means that within the considered model, the particles prefer to couple in pairs that contribute the energies u_{AA}, u_{BB}, or u_{AB} to the potential energy of the system (three upper rows in Table II). Obviously, if u_{BB} (u_{AA}) is the lowest pair energy, the B (A) patches face each other. In this case, the antiparallel orientation is favored. In contrast, when u_{AB} is the lowest pair energy, the head-to-tail configurations are the most profitable. These pairs corresponds roughly to the preferred configurations (ss, nn, sn) considered in the model of Erdman *et al.* [10]. Moreover, our model does not predict the occurrence of the polar phase with all particles aligned along one of the axes (the pairs x_{11}, x_{22}, y_{33}, y_{44} are energetically penalized). In contrast to the model of Janus fluids with up-down constrained orientations [8,9], there are no restrictions for the possible pair configurations.

TABLE II. The listing of investigated systems and corresponding values of parameters.

Code	u_{AA}	u_{BB}	u_{AB}	ε
M_1	−1	−1	0	−2
M_2	−1	−1	+1	−4
M_3	−1	−1	+2	−6
M_4	0	−1	−2	+3
M_5	0	−1	−1	+1
M_6	+2	−1	0	+1

We next consider the ordered structures formed by our Janus disks in two dimensions. The ordering in a given system depends on the relations between the energy parameters and space limitations in a dense fluid. In our model, the ground-state properties can be described using energies u_{AA} and u_{AB} for the fixed energy $u_{BB} = -1$. We define the parameter $\varepsilon = u_{AA} + u_{BB} - 2u_{AB}$ that dictates the type of ordered phase. If $\varepsilon < 0$, two SAF (quasilamellar) structures are observed. The SAF1 structure consists of alternating strips of particles in the orientations 1 and 2. These strips are oriented parallel to the x axis. However, the structure SAF2 corresponds to strips of particles in the states 3 and 4, aligned to the y axis. For $\varepsilon > 0$, the antiferromagnetic phases are formed. The AF1 (AF2) structure consists of particles in the orientations 1 and 2 (3 and 4), as shown in Fig 2. The regions of stability of the ordered phases are sketched in the ground-state phase diagram for the fully filled lattice (Fig. 3).

The structural transitions in our system resemble to some degree a demixing in a binary mixture. Both transitions are caused by the difference in strengths of interactions between

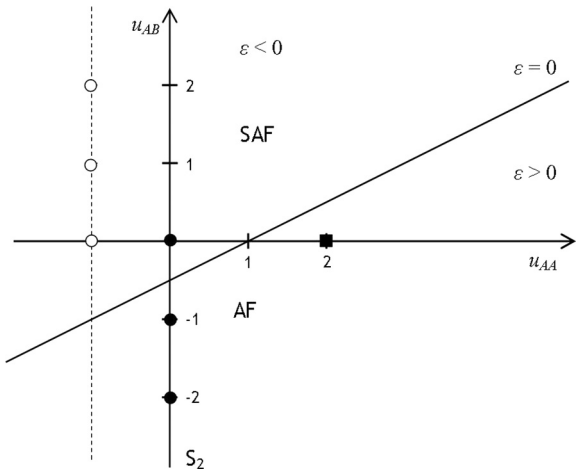

FIG. 3. Ground-state diagram for the system with $u_{BB} = -1$ at a fully filled lattice. Vertical dashed line corresponds to the same AA and BB interactions ($u_{AA} = -1$). The solid line ($\varepsilon = 0$) delimits the regions of the stability of the SAF and AF phases. Symbols show the points at which the calculations have been carried out.

similar and dissimilar moieties. One can treat the fluid of Janus disks as an equimolar mixture of halves A and B. However, in the considered particles these parts are permanently bonded. Thus, a change of the parameter ε can only cause changes in the orientations of particles. As a consequence, ordered structures with different numbers of energetically profitable and unprofitable contacts are formed.

If all interactions in the system are nonrepulsive, the model predicts that all possible ordered structures correspond to a fully covered lattice. On the other hand, when interactions are repulsive, ordered phases can be formed also for lower densities. We return to this problem later.

We want to scan systematically the space of model parameters. However, our goal is to show general trends in the phase behavior of the model rather than to consider details of phase diagrams of the investigated systems. We carried out a simulation for selected values of the energy parameters (see Table II). We chose the sets of parameters corresponding to those used in the previous studies of heterogeneous dimers [36–38], amphiphilic Janus particles [17], and symmetrical binary mixtures [54]. We show the analogies between the phase behaviors of these systems.

We consider two sets of the investigated systems. In the first group, AA and BB interactions are the same, $u_{AA} = u_{BB} = -1$ (systems M1–M3). For the second set of systems, these interactions are different and $u_{AA} = 0$, $u_{BB} = -1$ (systems M4–M6). The points corresponding to the studied systems are located at the vertical dashed line and at the u_{AB} axis in Fig. 3, respectively. Additionally, we considered the system with $u_{AA} = +2$, $u_{BB} = -1$, and $u_{AB} = 0$ (M7).

Now we discuss the behavior of the systems with the same AA and BB interactions, $u_{AA} = u_{BB} = -1$ (the dashed vertical line in the ground-state diagram drawn in Fig. 3). We performed simulations at points marked as void circles. This class of Janus particles corresponds to the heterogeneous dimers studied in our previous paper [36]. Note that for system M1, $u_{AB} = 0$, while for systems M2 and M3, AB interactions are repulsive. We have found that each system (M1–M3) underwent a first-order "condensation" from a colloidal-poor (gas) to a colloidal-rich (liquid) phase and a continuous transition from an isotropic fluid to the ordered fluid of the SAF type.

To shed more light on the nature of the observed transitions, we analyzed the histograms of the density and the histograms of the order parameters. The results are qualitatively the same for all investigated systems (M1–M3). At low temperatures, the density histograms are double-peaked distributions characteristic of first-order transitions [47]. We observe a coexistence between a colloidal-poor and a colloidal-rich phase that disappears above a critical temperature. For high temperatures, we obtained the Gaussian histograms of the density.

We also studied the transition from a disordered to an ordered phase. Figure 4 gives typical examples of the histograms of the order parameter Ψ_{SAF1} (or Ψ_{SAF2}). These results were obtained for the system M1. The histograms were estimated at the fixed temperatures $T^* = 0.5$, i.e., above the temperature range at which the first-order transition occurs, and different values of the chemical potential. For $\mu = -1.2$, the order parameter distribution Ψ_{SAF1} (the distribution Ψ_{SAF2} is the same) exhibits three maxima due to the SAF phase,

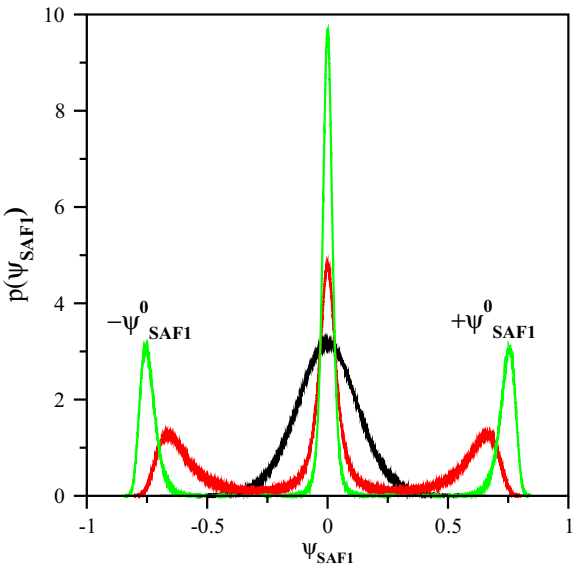

FIG. 4. (Color online) Distributions of the component Ψ_{SAF1} (the distributions of the component Ψ_{SAF2} are the same) of the order parameter Ψ_{SAF} for the system M1 obtained at $T^* = 0.5$ and $\mu^* = -1.200$ (green line), $\mu^* = -1.225$ (red line), and $\mu = -1.250$ (black line). The size of the simulation cell $L = 84$.

two at $\pm\Psi^0_{\mathrm{SAF1}}$ and one at $\Psi_{\mathrm{SAF1}} = 0$. The values $\pm\Psi^0_{\mathrm{SAF1}}$ are indicated in Fig. 4. Notice that the maximum at $\Psi_{\mathrm{SAF1}} = 0$ does not prove the presence of any disordered phase, but it is a consequence of the existence of differently oriented domains of the SAF phase, namely the structures SAF1 and SAF2. The order parameters Ψ_{SAF1} and Ψ_{SAF2} correspond to the domains oriented along two orthogonal directions, so it is not possible that both of them assume zero values. If one of these order parameters is close to zero, the other has a value close to $\pm\Psi^0_{\mathrm{SAF1}}$. As the chemical potential decreases, the maxima at $\pm\Psi^0_{\mathrm{SAF1}}$ are located closer to zero and become lower. Above the λ line ($\mu = -1.250$) there is a single-peak distribution corresponding to a disordered phase.

Next, we analyzed the changes of the order parameter Ψ_{SAF} and of its fourth cumulant, $U_L(\Psi_{\mathrm{SAF}})$, with temperature and the chemical potential. We concluded that the phase transition between a disordered fluid and the SAF phase is continuous.

The results obtained for systems M1–M3 are summarized in Fig. 5, which presents the phase diagrams in T-ρ (a) and T-μ (b) coordinates. Let us discuss some details of the phase diagram for the system M1 (nonrepulsive interactions). At very low temperatures, there is a coexistence between a disordered gas and the ordered, SAF-type liquid. In other words, there is a first-order transition between a disordered colloidal-poor and an ordered colloidal-rich SAF phase. For higher temperatures, there exists a line of critical points separating a disordered fluid and the ordered SAF fluid (λ line). This line corresponds to a continuous, structural transition. We have not found a coexistence between ordered and disordered liquid. The λ line can cross the gas-liquid coexistence envelope at the critical point of condensation (a tricritical point) or below the critical point at a critical end point. Above the critical temperature of "condensation," only the supercritical fluid exists, similarly to the phase diagram of a simple fluid.

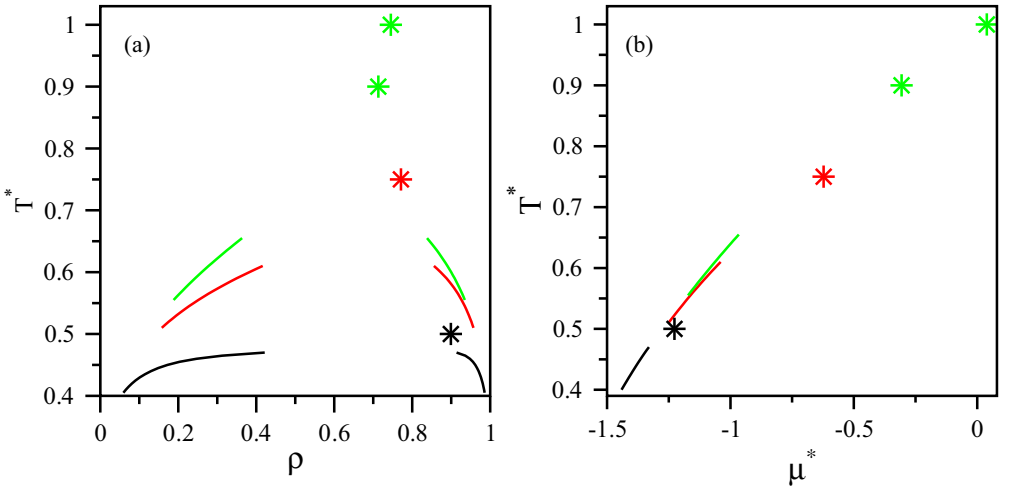

FIG. 5. (Color online) The density-temperature (a) and the chemical potential-temperature (b) projections of phase diagrams obtained for the following systems: M1 (black line), M2 (red line), and M3 (green line). Solid lines represent the first-order coexistence curves. The symbols are located on the λ lines corresponding to the second-order transitions to the SAF phase.

The phase diagrams obtained for the systems M3 and M3 have analogous topologies—with the vapor-liquid coexistence lines and λ lines corresponding to the second-order transition between disordered and ordered fluids. Unfortunately, we did not answer the question of whether the λ lines cross the coexistence envelope at the tricritical points or at the critical end points. We cannot also preclude that a change of u_{AB} changes the topology of the phase diagram from a diagram with a tricritical point to one with an end critical point. In the considered systems, the λ lines cross the coexistence envelopes very closely to the critical points. In such a situation, very strong fluctuations of the order parameters are observed. It is well known that a precise determination of the critical end point located near the condensation critical point is a difficult task [55–57]. The standard finite-size scaling techniques can be effectively used only for very large simulation cells. This makes simulations very time-consuming even for the two-dimensional (2D) lattice model. We want to show only the fundamental features of phase diagrams of different model systems. Therefore, we did not concentrate on this problem. Nevertheless, one sees how the phase diagram changes with increasing energy u_{AB}. In the considered case of nonattractive AB interactions, an increase of u_{AB} causes a rise of the critical temperature and the critical potential. Stronger repulsion between particles causes an increase in critical temperature. The reason for this striking behavior is the ordering of the colloidal-rich phase. At temperatures slightly lower than the critical temperature of "condensation," there is a coexistence between a disordered fluid and a highly ordered phase of the SAF type. The critical temperature depends on the ratio of energy and entropy differences between a fully disordered state and the ground state ($T = 0$) [58]. There are no AB contacts in a perfectly ordered SAF phase ($\Psi_{\mathrm{SAF}} = 1$). Therefore, at the ground state, the energy and entropy are independent of u_{AB}. In a disordered fluid, however, the mean energy increases with u_{AB}. As a result, the critical temperature also increases.

In Table III, we give the locations of the second-order transitions and the fixed point values of the fourth-order cumulants $U^*(\Psi)$ at the transition points, estimated for selected thermodynamic conditions. The results obtained for the systems M1–M3 demonstrate that the structural transition to the SAF phase is nonuniversal, as expected.

It is instructive to compare the phase diagrams obtained for the systems M1–M3 with the phase diagrams estimated for similar, physical systems. As has been mentioned, the SAF-type phases were observed either in magnets or in heterogeneous dimers. The order parameter Ψ_{SAF} has been used to describe ordering in these systems. In the case of heterogeneous dimers, the ordered SAF fluid (lamellar) was found [36]. The alternating strips of A and B segments are formed by dimers lying parallel to the x or y axes. The AB dimers seem to be very similar to Janus disks. However, the anisotropy of the shape can strongly affect the self-organization processes. Moreover, in the lattice model a dimer occupies two lattice sites. As a consequence, there is no statistical equivalence between particles and vacancies. The occupation of a given site ensures that one of its nearest neighbors is also occupied. The configurational entropies of the same number of heterogeneous dimers and Janus disks are considerably different. Phase equilibrium is established on the basis of compensation between the internal energy and entropy. Therefore, the phase diagrams of Janus disks and the

TABLE III. The location of (T^*,μ^*) the second-order phase transitions in the investigated systems. Columns 4 and 5 give the fixed-point values of the fourth cumulants of the suitable order parameters.

Code	T^*	μ^*	$U^*(\Psi_{\mathrm{SAF}})$	$U^*(\Psi_{\mathrm{AF}})$
M_1	0.500	−1.2267	0.625	
M_2	0.750	−0.6224	0.606	
M_3	0.900	−0.3066	0.600	
	1.000	0.0390	0.6001	
M_4	0.829	−2.5000		0.638
	0.839	−2.0000		0.638
M_5	0.282	−1.5000		0.637

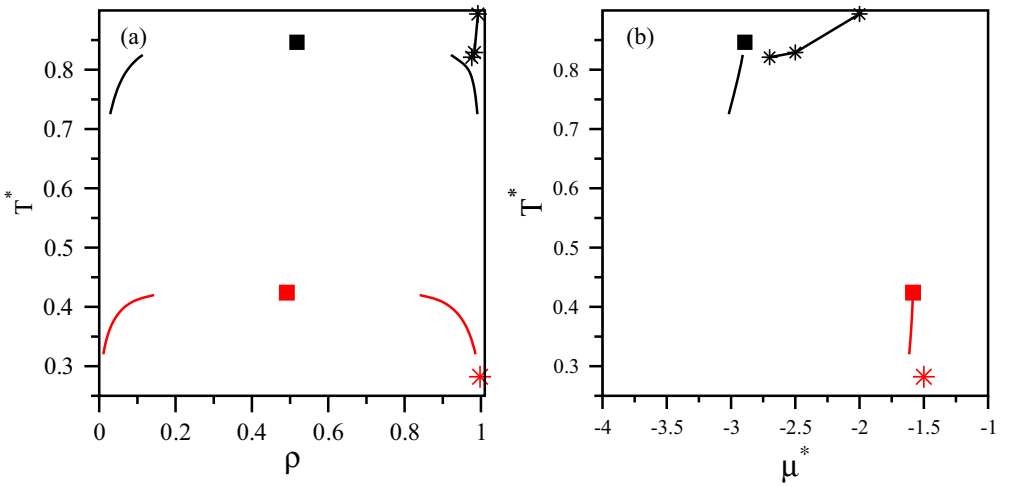

FIG. 6. (Color online) The density-temperature (a) and the chemical potential-temperature (b) projections of phase diagrams obtained for the systems M4 (black lines) and M5 (red lines). Solid lines represent the first-order coexistence curves. The symbols are located on the λ lines corresponding to the second-order transitions to the AF phase.

heterogeneous dimers interacting in a similar way can exhibit a different topology, such as, for example, the phase diagram for the system M1 and for dimers (see Fig. 1 in Ref. [36]).

However, the phase diagrams presented in Fig. 5 have the same topology as the phase diagram estimated for the symmetrical binary mixtures of Lennard-Jones fluids, in which there is a vapor-liquid coexistence line and the λ line corresponding to a continuous transition between the mixed and demixed fluid (see Fig. 4 in Ref. [54]).

Now we turn to the model with different AA and BB interactions, which is likely better suited to describe proper Janus particles than that considered above. We discuss here the results obtained for systems M4–M6 (points on the u_{AB} axis, marked as filled circles in Fig. 3). In this case, $u_{BB} = -1$, $u_{AA} = 0$, whereas AB interactions are nonrepulsive. We again investigate how an increase in the pair energy u_{AB} affects the phase behavior of the system. As predicted, we found the AF-type structures in the systems M4 ($u_{AB} = -2$) and M5 ($u_{AB} = -1$), while for the system M6 ($u_{AB} = 0$) the SAF ordering was found. We have shown that the systems M4 and M5 underwent first-order "condensation" and a continuous phase transition between a disordered fluid and the AF phase.

The resultant phase diagrams for the systems M4 and M5 are shown in Fig. 6. One sees that the systems M4 and M5 underwent first-order "condensation" and a continuous phase transition between a disordered fluid and the AF phase. As in the previous case, at very low temperatures there is a coexistence between a disordered gas and the ordered liquid. However, the structure of this ordered liquid is different. The λ lines attain the coexistence curves at the critical end points. This means that at temperatures slightly below the critical temperature, the coexistence between two disordered phases of distinct densities is observed. We have here an "usual condensation."

Using the standard finite-size scaling methods described in the preceding section, we estimated the following critical parameters: $T_c^* = 0.8464$, $\mu_c^* = -2.892\,24$, and $\rho_c = 0.517\,95$ for system M4, and $T_c^* = 0.424$, $\mu_c^* = -1.584\,28$, and $\rho_c = 0.491\,60$ for system M5. The fixed-point value of the

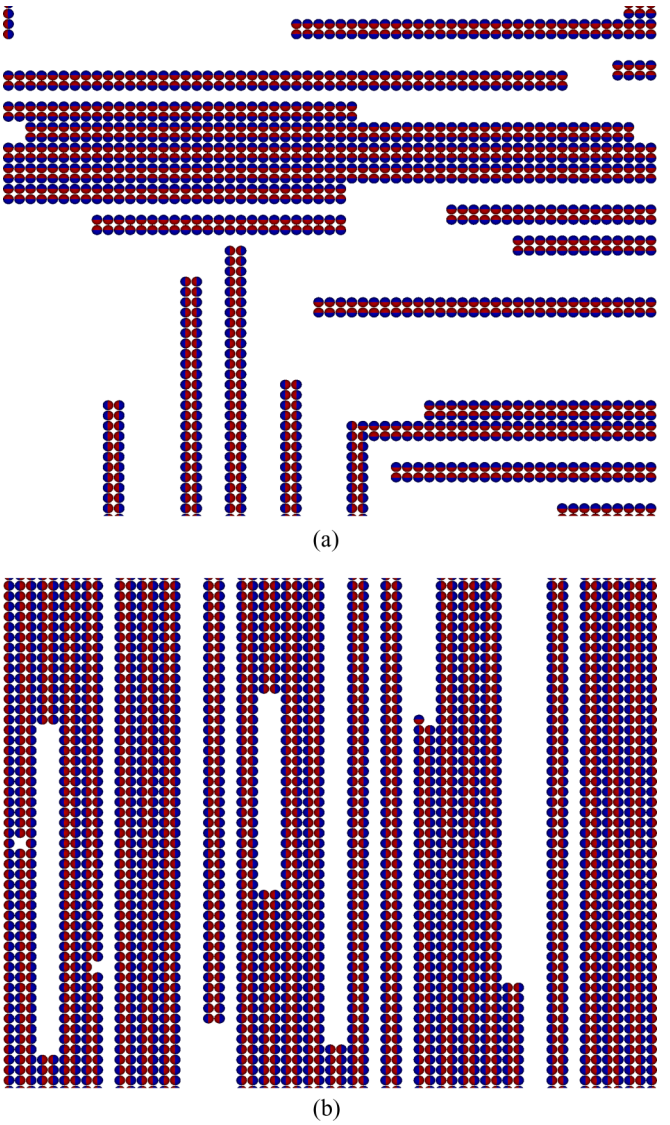

FIG. 7. (Color online) Fragments of snapshots of configurations recorded for M6 at $T^* = 0.1$ and $\rho = 0.4$ (a) and $\rho = 0.7$ (b); $L = 192$.

fourth-order cumulant of the order parameter m is equal to $U_m^* \approx 0.615$. This confirms that the condensation transition belongs to the universality class of the 2D Ising model. As one can expect, with weakening AB attraction the critical temperature of "condensation" decreases since the total strength of attraction decreases. At the same time, the critical chemical potential increases while the critical density shows only a slight decrease. Moreover, the λ line attains the coexistence curve at a considerably lower temperature. It is interesting that the structural transition to the AF phase is nonuniversal (see Table III).

In our earlier works [37,38], we studied heterogeneous dimers with different AA and BB interactions. These dimers formed an ordered phase similar to the AF structure shown in Fig. 2. The order-disorder transition was continuous. We found that depending on the strength of the AA interactions, the λ line crossed the coexistence envelope at the tricritical point or at the critical end point [38].

A markedly different situation was encountered in the case of $u_{AB} = 0$ (M6). Because $\varepsilon = -1$, the SAF-type structures should be formed. Notice that now only pairs of particles connected via B patches or their parts contribute to the potential energy of the system ($u_2 = u_{BB}$ and $u_4 = u_6 = u_{BB}/2$ in Table I).

The model system M6 corresponds, to some extent, to the Janus particles studied by Sciortino *et al.* [12]. Within their model, each particle consists of one attractive patch (say B) and the other part, which only induces steric repulsion. In lattice models, the particles located on neighboring sites cannot overlap, so the steric repulsion is an immanent feature of the model. There are no attractive AA and AB interactions, either in our M6 model or in the model of Sciortino and co-workers [12]. However, one should remember that the symmetry of the lattice and the restrictions of the particle orientations change the behavior of our system.

At high temperatures, the fluid is completely disordered. Upon decreasing temperature, these interactions become more and more important. As a consequence, particles start to connect into clusters. In the system M6, we observe a strong tendency of the particles to aggregate in the "SAF-type" bilayers that expose to the outside only neutral parts A. Such "double chains" are formed even at low fluid densities. Similar

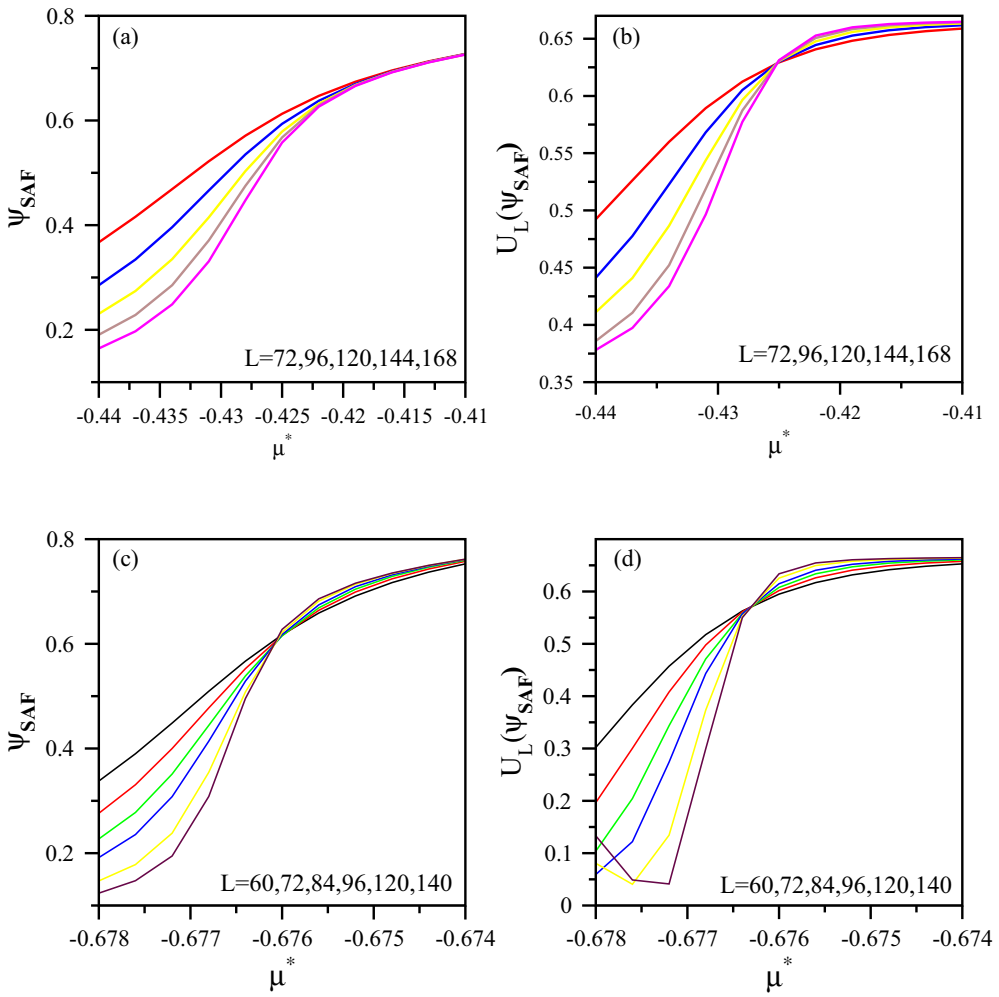

FIG. 8. (Color online) The results for the system M6. Changes of the order parameter Ψ_{SAF} with the chemical potential (a,c) and the corresponding changes of the fourth-order cumulant $U_L(\Psi_{SAF})$(b,d) obtained at $T^* = 0.25$ (a,b) and $T^* = 0.2$ (c,d). The calculations have been carried out for the different sizes of the simulation cell, $L = 60$ (black lines), 72 (red lines), 84 (green lines), 94 (blue lines), 120 (yellow lines), 140 (maroon lines), 144 (brown lines), and 168 (magenta lines).

aggregates were formed in the Janus particles interacting via the Kern-Frenkel potential [12]. Examples of snapshots are presented in Fig. 7(a). However, there is no energetic profit connected with the sticking of the aggregates. The self-organization prevents the demixing of the system into colloidal-poor (gas) and colloidal-rich (liquid) phases. We see the competition between self-assembly and "condensation." Nevertheless, at low temperatures [Fig. 7(b)], a kind of "droplet" (thick ordered layers) is visible.

We now turn to the question of whether there is a first-order gas-liquid transition in the system in hand. The results of grand canonical simulation were rather striking. Even at very low temperature, the density probability distribution had a single peak. This suggests the existence of only one phase. However, an analysis of the order parameter Ψ_{SAF} and its fourth cumulant led to the opposite conclusion. Figure 8 presents the plots of the changes of the order parameter Ψ_{SAF} as well as of the four-order cumulant $U_L(\Psi_{SAF})$ with the chemical potential at two temperatures, $T^* = 0.25$ [Figs. 8(a) and 8(b)] and $T^* = 0.2$ [Figs. 8(c) and 8(d)]. Indeed, inspecting the data in Fig. 8, one notes that the curves in parts (a) and (b) are typical for second-order transitions. However, at lower temperature, $T = 0.2$, the behavior of either the order parameter or of its cumulant is characteristic of the first-order transition. In particular, the order parameters calculated for different sizes of the simulation cell exhibit a crossing point. Moreover, for sufficiently large systems, the corresponding cumulants show the presence of minims. These observations confirm the appearance of a first-order transition between a disordered and an ordered SAF phase in the system M6. Unfortunately, we could not determine the densities of the coexisting phases.

To confirm the fluid-fluid coexistence, we have carried out simulations in a canonical ensemble. An important result is evident from Fig. 9. At $T^* = 0.1$, $\rho = 0.6$ after an extremely long equilibration, we have found almost a two-peaked distribution of probability. Taking into account all the results, we suppose that there is a first-order transition between an isotropic colloidal-poor fluid and the ordered colloidal-rich SAF phase. We have not found the reentrant transition in this system [12].

Finally, we want to present the selected results for the system M7, $u_{AA} = +2$, $u_{AB} = 0$, which can mimic a two-dimensional fluid of simple amphiphile particles. The patches A are hydrophilic, whereas the patches B can be considered as hydrophobic. The energetic preference (or penalty) of configurations with facing B parts (or A parts) corresponds to amphiphiles in aqueous solutions. The water molecules accumulate near the hydrophilic side A. The resulting steric exclusion leads to an effective repulsion between hydrophilic patches A of amphiphilic particles. The model M7 is qualitatively similar to that proposed by Rosenthal and Knapp [21].

The behavior of the system M7 is in contrast to what was found in the remaining cases. We have seen no evidence of a vapor-liquid transition in the fluid. At the same time, we have observed various self-organization processes.

In this case, AA interactions were strongly repulsive. Therefore, for low surface coverage, the formation of aggregates that expose to the outside the parts A is energetically preferred. At very low temperatures, one can expect that the dimers with two B patches facing each other appear in the system (pairs x_{34},y_{12}). Another favorite cluster consists of four particles with B parts oriented to the aggregate center. Examples of such clusters are presented in Figs. 10(a) and 10(b). The systems

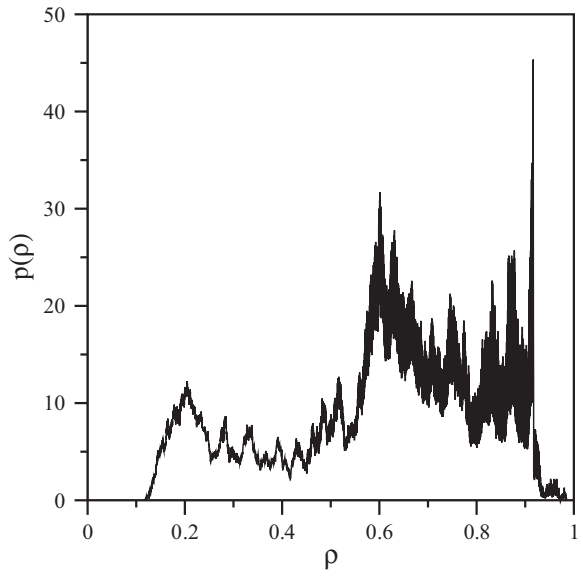

FIG. 9. The block density probability distribution for the system M6 at temperature $T^* = 0.1$ and $\rho = 0.6$ density. The system size $L = 192$ and the block size $L_b = 48$.

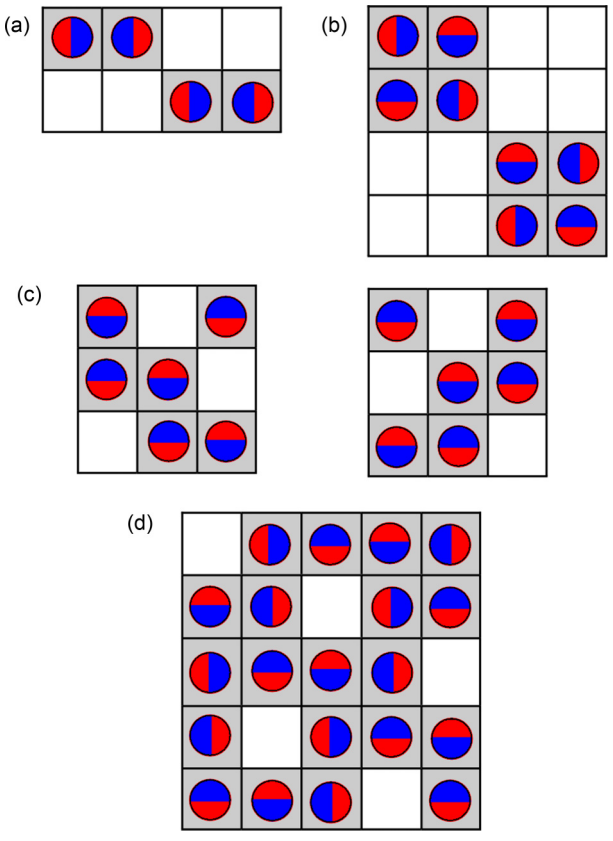

FIG. 10. (Color online) Schematic representation of possible ordered structured at low and medium densities in the monolayer: (a) dimers, (b) "micelles," (c) zigzag structures at $\rho = 2/3$, and (d) S-structure ($\rho = 4/5$).

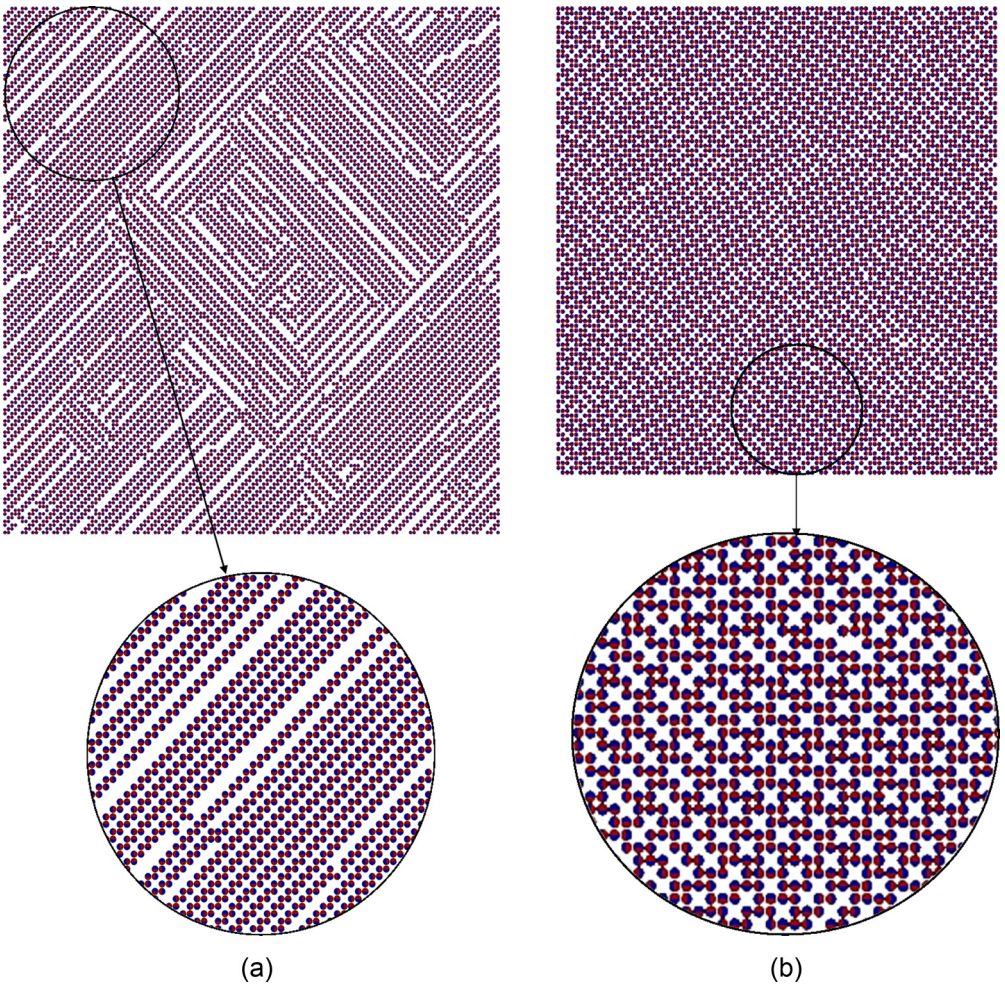

FIG. 11. (Color online) Fragments of snapshots of configurations recorded for M7 at $T^* = 0.025$ and $\rho = 0.573$ (a) and for $T^* = 0.1$, $\rho = 0.763$ (b).

containing the dimers or the "micelles" have the same energy per lattice site, namely $E = -0.25$. One can easily show that the dimers linked in the zigzag pattern [see Fig. 10(c)] correspond to the lowest energy $E = -0.33$. Notice that the energetic differences between these structures are rather small.

At the ground, the AF phase is stable for a fully covered lattice. However, dominating repulsive interactions cause the emergence of various ordered structures at medium densities of the monolayer. These structure have lower energy per particle than the AF phase. We found stable structures at $\rho = 2/3$ and $4/5$. It is interesting that there are well-pronounced patterns built out of occupied and empty sites. The orientations of the particles in such structures can be different. A great number of configurations correspond to the same energy of the system. Moreover, the differences between energies calculated from different configurations are not significant.

At $\rho = 2/3$, the zigzag structures appear in the monolayer. There are sloping steplike strips of occupied sites. The lattice sites between these strips remain empty. Examples of zigzag structures with favorite orientations of particles are shown in Fig. 10(c).

Figure 10(d) illustrates an example of an ordered structure that can be formed at $\rho = 4/5$. Also in this case, the pattern of occupied and empty sites is well visible. One sees here the zigzag structure built of "micelles" composed of four occupied sites (S structure). In such an ordered phase, particles can be differently oriented. The lowest energy level is highly degenerated.

At temperatures $T^* > 0$, the equilibrium configuration is the result of the energetic and entropic balance in the system. We have inspected the snapshots for selected thermodynamic conditions. The evolution of the system structure with increasing density is shown in Fig. 11. As expected, we found domains of differently oriented zigzag structures at $\rho = 0.573$ [Fig. 11(a)]. For the denser monolayer ($\rho = 0.763$), however, we see patches of various S structures [Fig. 11(b)]. The considered system can self-organize into various structures depending on the density and temperature.

V. CONCLUSIONS

This paper presents the results of Monte Carlo simulation of Janus disks on a square lattice. The Janus particles, consisting of two halves, A and B, interacted via a short-ranged directional potential. We have formulated a simple model for directional interactions between the particles. Four possible orientations of a particle on a given lattice site were considered. The interactions between neighboring particles depended on

their orientations. To control the strength of the interactions, we have used only three energy parameters—u_{AA}, u_{BB}, and u_{AB}—that characterized AA, BB, and AB contacts. The two first parameters correspond to particles that point with their A (B) patches toward each other, while u_{AB} is the pair energy of the head-to-tail configuration. The energy of any possible configuration was assumed to be an arithmetic average of two energy parameters. Based on that model, we were able to study the phase behavior of the system for different sets of energy parameters.

First, we discuss the ordered structures that can appear in the model. In the limiting case of a fully filled lattice ($\rho = 1$), we have found two ordered structures, SAF and AF. The occurrence of these phases depends on the relations between the energy parameters. We have analyzed the ground-state phase diagram in the coordinates $u_{AA} - u_{BB}$. In this diagram, the line $\varepsilon = u_{AA} + u_{BB} - 2u_{AB} = 0$ delimits the regions of stability of both phases (see Fig. 3). For lower fluid densities ($\rho < 1$), SAF and AF structures with vacancies are formed. The model predicts other ordered structures when at least one of the energy parameters is positive (repulsive interactions) at $\rho = 1/2$ (all repulsive interactions [59]), $\rho = 2/3$ (zigzag phase), and $\rho = 4/5$ (S phase).

The second question concerned the nature of phase transitions in selected model systems. We considered two types of model systems. For the first group, interactions between the same parts of particles were assumed to be identical (M1–M3). The other group mimics the "proper" Janus particles with different AA and BB interactions (M4–M6). We have considered the influence of the parameter on the phase behavior of the model systems.

In systems M1–M5, we found two phase transitions: a first-order "condensation" from a colloidal-poor (gas) to a colloidal-rich (liquid) phase, and a continuous transition from a disordered fluid to the ordered fluid. As expected, we found the SAF phase for the systems M1–M3 and the AF structure for the systems M4 and M5. Using finite-size scaling theory, we estimated the location of the order-disorder transition for the selected thermodynamic conditions (λ line). We found that for the systems M4 and M5, the λ lines cross the coexistence envelope at the critical end points.

We also discussed the evolution of the phase diagram topology due to changes of the parameters. In the first group of model systems, the repulsive AB interactions were considered. In this case, an increase of u_{AB} causes a rise of the critical temperature and the critical potential. Different effects are observed for the second group of investigated systems. When the AB interactions were assumed to be attractive, an increase of u_{AB} led to a decrease of the critical temperature while the critical chemical potential increased.

We suppose that for fixed values of the energy parameters u_{AA} and u_{BB}, a change of u_{AB} can change the topology of the phase diagram from a diagram with a tricritical point to one with an end critical point. However, the solution of this problem was beyond of the scope of this work. We have shown that structural transitions to either SAF or AF phase are nonuniversal.

A very interesting behavior is observed for the system M6 ($u_{AA} = 0, u_{BB} = 0$). These particles exhibit a strong tendency to aggregate in the "SAF-type" bilayers, which expose to the outside only neutral parts A. This prevents any attraction between distinct clusters, so the formation of droplets is difficult. One can say that the self-organization competes with the demixing of the system into a colloidal-poor (gas) and colloidal-rich (liquid) phases. However, we have shown that the system M6 underwent first-order "condensation" at very low temperatures.

Other significant results were obtained for the system M7 ($u_{AA} = +2$, $u_{AB} = 0$). In that case, we did not find first-order "condensation." However, we observed various self-organization processes. Strong repulsive AA interactions together with the BB-attractive interactions cause the emergence of various ordered structures at medium densities of the monolayer. These structures can be considered as patterns built out of occupied and empty lattice sites. In a given structure, orientations of particular particles can be different. Numerous configurations correspond to the same energy of the system. The entropy additionally stabilizes the structure. We found two types of ordered phases, namely zigzag structures ($\rho = 2/3$) and S structures ($\rho = 4/5$). Self-organization into highly ordered large clusters prevent "condensation." This effect was also reported by Sciortino *et al.* [12].

In summary, we introduced a simple model capable of predicting the collective behavior of various Janus disks in monolayers. This model generates different types of self-assembly and phase transitions. The main advantage of the model is that it can be easily adapted to study different systems. Moreover, its application reduces the computation time considerably. The results provide guidance for further study of concrete systems in the framework of more realistic models.

ACKNOWLEDGMENTS

This work is supported by European Commission Research Executive Agency under Grant No PIRSES-GA-2010-268498. We thank. J. Ilnytskyi for stimulating discussions.

[1] J. Hu, S. Zhou, Y. Sun, X. Fang, and L. Wu, Chem. Soc. Rev. **41**, 4356 (2012).
[2] Z. Zhang and S. C. Glotzer, Nano Lett. **4**, 1407 (2004).
[3] C. Casagrande, P. Fabre, E. Raphael, and M. Veyssie, Europhys. Lett. **9**, 251 (1989).
[4] F. Schmid, in *Computational Methods in Surface and Colloid Science*, edited by M. Borówko, Surface Series Vol. 89 (Dekker, New York, 2000).
[5] A. Walther, X. Andre, M. Drechsler, V. Abetz, and A. H. E. Mueller, J. Am. Chem. Soc. **129**, 6187 (2007).
[6] G. Munao, P. O'Toole, T. S. Hudson, D. Costa, C. Caccamo, A. Giacometti, and F. Sciortino, Soft Matter **10**, 5269 (2014).
[7] D. J. Kraft, R. Ni, F. Smallenburg, M. Hermes, K. Yoon, D. A. Weiz, A. van Blaaderen, J. Groenewold, M. Dijkstra, and K. Kegel, Proc. Natl. Acad. Sci. (USA) **109**, 10787 (2012).
[8] M. A. G. Maestre, R. Fantoni, A. Giacometti, F. Sciortino, and K. Dawson, J. Chem. Phys. **138**, 094904 (2013).
[9] R. Fantoni, A. Giacometti, M. A. G. Maestre, and A. Santos, J. Chem. Phys. **139**, 174902 (2013).

[10] T. Erdmann, M. Kröger, and S. Hess, Phys. Rev. E **67**, 041209 (2003).
[11] N. Kern and D. Frenkel, J. Chem. Phys. **118**, 9882 (2003).
[12] F. Sciortino, A. Giacometti, and G. Pastore, Phys. Rev. Lett. **103**, 237801 (2009).
[13] F. Sciortino, A. Giacometti, and G. Pastore, Phys. Chem. Chem. Phys. **12**, 11869 (2010).
[14] T. Vissers, Z. Preisler, F. Smallenburg, M. Dijkstra, and F. Sciortino, J. Chem. Phys. **138**, 164505 (2013).
[15] A. G. Vanakaras, Langmuir **22**, 88 (2006).
[16] D. Salgado-Blanco and C. I. Mendoza, Eur. Phys. J. E **36**, 38 (2013).
[17] G. Rosenthal, K. E. Gubbins, and S. H. L. Klapp, J. Chem. Phys. **136**, 174901 (2012).
[18] H. Schmidle, C. K. Hall, O. D. Velev, and S. H. L. Klapp, Soft Matter **8**, 1521 (2012).
[19] M. M. Moghani and B. Khomami, Soft Matter **9**, 4815 (2013).
[20] G. Gompper and M. Schick, in *Phase Transitions and Critical Phenomena*, edited by C. Domb and J. L. Lebowitz (Academic, London, 1994), Vol. 16.
[21] G. Rosenthal and S. H. L. Klapp, J. Chem. Phys. **134**, 154707 (2011).
[22] G. Rosenthal and S. H. L. Klapp, Int. J. Mol. Sci. **13**, 9431 (2012).
[23] M. Borówko, T. Poeschel, S. Sokołowski, and T. Staszewski, J. Phys. Chem. B **117**, 1166 (2013).
[24] A. Giacometti, F. Lado, J. Largo, G. Pastore, and F. Sciortino, J. Chem. Phys. **131**, 174114 (2009).
[25] A. Giacometti, C. Goegelein, F. Lado, F. Sciortino, and G. Pastore, J. Chem. Phys. **140**, 094104 (2014).
[26] G. Goegelein, F. Romano, F. Sciortino, and A. Giacometti, J. Chem. Phys. **136**, 094512 (2012).
[27] F. Bresme and M. Oettel, J. Phys.: Condens. Matter **19**, 413101 (2007).
[28] S. Kinge, M. Crego-Calama, and D. Reinhoudt, ChemPhysChem **9**, 20 (2008).
[29] D. L. Cheung and S. A. F. Bon, Soft Matter **5**, 3969 (2009).
[30] T. M. Ruhland, A. H. Groeschel, N. Ballard, T. S. Selhon, A. Walther, A. H. E. Mueller, and A. F. Bon, Langmuir **29**, 1388 (2013).
[31] A. Walther and A. H. E. Mueller, Soft Matter **4**, 663 (2008).
[32] S. Loi, U. M. Wiesler, H. J. Butt, and K. Mullen, Macromolecules **34**, 3661 (2001).
[33] S. Loi, H. J. Butt, C. Hampel, R. Bauer, and K. Mullen, Langmuir **18**, 2398 (2002).
[34] C. J. Xia, X. W. Fan, J. Locklin, R. C. Advincula, A. Gies, and W. Nonidez, J. Am. Chem. Soc. **126**, 8735 (2004).
[35] A. Patrykiejew, S. Sokołowski, and K. Binder, Surf. Sci. Rep. **37**, 207 (2000).
[36] W. Rżysko and M. Borówko, J. Chem. Phys. **117**, 4526 (2002).
[37] W. Rżysko and M. Borówko, Surf. Sci. **520**, 151 (2002).
[38] W. Rżysko and M. Borówko, Surf. Sci. **600**, 890 (2006).
[39] W. Rżysko, A. Patrykiejew, and K. Binder, Phys. Rev. B **72**, 165416 (2005).
[40] W. Rżysko, A. Patrykiejew, and K. Binder, Phys. Rev. B **76**, 195409 (2007).
[41] K. Binder and D. P. Landau, Phys. Rev. B **21**, 1941 (1980).
[42] K. Binder, Phys. Rev. Lett. **47**, 693 (1981).
[43] G. M. Bell and D. A. Levis, *Statistical Mechanics of Lattice Models, Closed Form and Exact Theories of Cooperative Phenomena* (Wiley, New York, 1989), Vol. 1.
[44] M. Blume, V. J. Emery, and R. B. Griffiths, Phys. Rev. A **4**, 1071 (1971).
[45] D. Frenkel and B. Smit, *Understanding Molecular Simulations from Algorithms to Applications* (Academic, San Diego, 1996).
[46] J. J. de Pablo, Q. Yan, and F. A. Escobedo, Annu. Rev. Phys. Chem. **50**, 377 (1999).
[47] Q. Yan and J. J. de Pablo, J. Chem. Phys. **111**, 9509 (1999).
[48] D. P. Landau and K. Binder, *A Guide to Monte Carlo Simulation in Statistical Physics* (Cambridge University Press, Cambridge, 2000).
[49] A. M. Ferrenberg, in *Condensed Matter Physics III*, edited by D. P. Landau, K. K. Mon, and M. B. Schutter (Springer, Heidelberg, 1991).
[50] A. M. Ferrenberg and R. H. Swendsen, Phys. Rev. Lett. **61**, 2635 (1988).
[51] K. Binder, Z. Phys. B **43**, 119 (1981).
[52] M. Rovere, D. W. Hermann, and K. Binder, Europhys. Lett. **6**, 585 (1988).
[53] *Finite Size Size Scaling and Numerical Simulation of Statistical Systems*, edited by V. Privman (World Scientific, Singapore, 1990).
[54] N. B. Wilding, F. Schmid, and P. Nielaba, Phys. Rev. E **58**, 2201 (1998).
[55] K. Binder, in *Computational Methods in Field Theory*, edited by H. Gausterer and C. B. Lang (Springer-Verlag, Berlin, 1992).
[56] N. B. Wilding and P. Nielaba, Phys. Rev. E **53**, 926 (1996).
[57] N. B. Wilding, Phys. Rev. Lett. **78**, 1488 (1997).
[58] F. Roma, A. J. Ramirez-Pastor, and J. L. Riccardo, Phys. Rev. B **68**, 205407 (2003).
[59] A. J. Ramirez-Pastor, J. L. Riccardo, and V. Pereyra, Surf. Sci. **411**, 294 (1998).